nature biotechnology

BRIEF COMMUNICATION

https://doi.org/10.1038/s41587-020-00753-y

Left-handed DNA-PAINT for improved super-resolution imaging in the nucleus

H. J. Geertsema[1], G. Aimola[2], V. Fabricius[1], J. P. Fuerste[1], B. B. Kaufer[2] and H. Ewers[1]✉

DNA point accumulation in nanoscale topography (DNA-PAINT) increases the resolution and multiplexing capabilities of super-resolution imaging, but cellular DNA interferes with DNA–DNA hybridization between target and probe in the nucleus. Here, we introduce left-handed DNA (L-DNA) oligomers that do not hybridize to natural right-handed DNA (R-DNA) and demonstrate that L-DNA-PAINT has the same specificity and multiplexing capability as R-DNA-PAINT, but improves the imaging of nuclear targets by substantially reducing background signal.

Super-resolution microscopy techniques facilitate imaging of cellular structures down to the level of molecular detail. In single-molecule localization super-resolution microscopy (SMLM) techniques, nanometer-level resolution is achieved by sequential imaging of a large number of single molecules at nanometer-scale resolution, a few molecules at a time[1–3]. Different approaches have been developed to keep the majority of molecules dark while a small fraction are imaged as single molecules. The fluorescent proteins and organic dyes commonly used are physically or chemically switched between dark and bright states to separate detection events. Recently, DNA-PAINT[4] was developed as an approach that relies on the transient hybridization of fluorophore-coupled DNA oligomer imagers to target-associated, reverse-complement DNA oligomer binders. Since single-molecule detection occurs here through DNA hybridization and is uncoupled from dye photophysics, DNA-PAINT allows the use of bright, photostable organic dyes to obtain maximal single-molecule localization resolution[4,5]. Furthermore, different oligomer sequences enable multiplexing in a single wavelength[4,6], thereby avoiding chromatic aberration[7]. Finally, the well-understood chemical kinetics of DNA hybridization facilitate quantitative imaging[8,9]. In the light of these advantages, DNA-PAINT is an important advancement in single-molecule localization microscopy.

However, any DNA-nonamer[4] has statistically, on average, 22,000 complementary binding sites in the diploid ~3-gigabase human genome that can contribute to false-positive hybridization events. In addition, the transcriptome may also contribute to undesired DNA–RNA hybridizations. This is a substantial problem in a super-resolution technique based on single-molecule localizations, which is one of the most promising approaches to advancing our understanding of the nanoscopic functional organization of the nucleus, an area of intensive research in cell biology[10–12]. To overcome this problem, here we employed oligomers synthesized from L-DNA for DNA-PAINT. L-DNA has physicochemical properties identical to those of generic R-DNA (Fig. 1a and Extended Data Fig. 1), but does not naturally occur and cannot hybridize with R-DNA (Fig. 1b)[13]. We hypothesized that L-DNA-PAINT would elicit less background in super-resolution imaging of nuclear targets than traditional R-DNA-PAINT.

We first addressed whether the performance of L-DNA-PAINT is comparable to that of R-DNA-PAINT. To do so, we visualized microtubule structures in HeLa cells and found that R- and L-DNA-PAINT performed equally well in resolving microtubules as hollow structures in the cytoplasm. The obtained average spacing of 39 ± 4 nm (mean ± s.d., $n = 9$) and 33 ± 6 nm (mean ± s.d., $n = 22$) between the two sides of the hollow structure, respectively (Fig. 1c), agrees well with previous reports[14]. Analysis of the resolution achieved by Fourier ring correlation[15] yielded a resolution of 33 and 39 nm for L- and R-DNA-PAINT, respectively. As such, we concluded that L-DNA matches the performance of R-DNA in DNA-PAINT.

Next, we investigated the hybridization potential of R-DNA imagers for genomic DNA by adding fluorescently labeled R-DNA imagers (P3) to fixed HeLa cells, in the absence of R-DNA binders. It immediately became apparent that the localization density (localizations per μm^{-2}) of fluorescent imagers in the nucleus was higher than in the cytoplasm of the cells (Fig. 1d). In contrast, when we subsequently exchanged R-DNA imagers for L-DNA imagers with the same nucleotide sequence (LP3) and in the same cell, localizations in the nucleus were reduced to the background level in the cytoplasm (Fig. 1d). Since the localization density of single imagers is highly dependent on the local imager concentration, we represent the ratio of localization density in the nucleus (caused by hybridizations between cellular DNA and imagers) over the cytoplasm (background localizations). We found that detections of the R-DNA imager P3 were substantially enriched in the nucleus (2.7 ± 0.4 (mean ± s.e.m.)-fold; Fig. 1e), but detections of the L-DNA imager LP3 were not. Further investigation of several other imager sequences confirmed the enhanced nuclear binding of R-DNA imagers and showed that this enhancement was independent of the fluorophore coupled to the imager (Fig. 1e and Extended Data Fig. 2). Whether we performed this experiment by first using R-DNA and then switched for L-DNA or the other way around, in both cases R-DNA imagers led to higher nuclear background than L-DNA imagers (Extended Data Fig. 3).

We expect false-positive localizations of R-DNA to be especially detrimental in assays where the cellular DNA is denatured and single DNA strands are exposed to hybridization by R-DNA imagers. Such assays are widely used for the investigation of DNA organization in the nucleus. One prominent example is the investigation of DNA replication sites by the incorporation of the non-natural nucleotide BrdU into the cell's chromosomes. We performed such an assay and stained incorporated BrdU with antibodies that were coupled to an equal mixture of R-DNA binder (B3) and L-DNA binder (LB3). Cells were imaged first in the presence of 1 nM P3,

[1]Institute of Chemistry and Biochemistry, Department for Biology, Chemistry and Pharmacy, Freie Universität Berlin, Berlin, Germany. [2]Institute of Virology, Department of Veterinary Science, Freie Universität Berlin, Berlin, Germany. ✉e-mail: helge.ewers@fu-berlin.de

washed and subsequently imaged again in the presence of 1 nM LP3. We found that cells exhibited a prohibitive level of background when incubated with P3, but allowed for specific and super-resolved detection of replication centers in the same cell when incubated with LP3 (Fig. 2a,b). We concluded that L-DNA-PAINT enables previously inaccessible experimental assays targeting cellular replication sites in cells.

An important advantage of DNA-PAINT is the ability to visualize multiple targets in a sample through multiplexing, avoiding chromatic aberration. When we performed L-DNA-PAINT against immunostained proliferating cell nuclear antigen (PCNA) and Ki67 in the nuclei of HeLa cells using different L-DNA imager–binder pairs (LP3–LB3 and LP12–LB12, respectively), we found discrete staining for both molecules consistent with their respective reported localization in the nucleus (Fig. 2c)[16].

To further validate our results, we performed fluorescence in situ hybridization (FISH), the assay used most frequently to investigate genomic localization, coupled with our DNA-PAINT approach. We used previously characterized HEK293T cells, infected with ubiquitous human herpesvirus 6 A (HHV-6A) and thus harboring two copies of the integrated HHV-6 into the telomeres of the host chromosomes (Extended Data Fig. 4)[17], to test the specificity of the L-DNA-PAINT technique in the nucleus.

Viral DNA was labeled with an HHV-6A-specific probe as described previously[18], which was then coupled in equimolar ratio with an L-DNA and an R-DNA binder (LB3 and B3). When we then added P3 imager strands for R-DNA-PAINT, we found a strong nuclear background as shown above. On the other hand, subsequent imaging with LP3 after washout resulted in discrete, super-resolved staining of the HHV-6 integration sites (Fig. 2d and Extended Data Fig. 5).

Taken together, we have demonstrated here that L-DNA-PAINT has the same specificity, resolution and multiplexing capabilities as traditional R-DNA-PAINT. Strikingly, we find that L-DNA-PAINT exhibits a drastically lower false detection rate and facilitates the investigation of structures and events pertaining to cellular DNA in the nucleus. Increased background in R-DNA-PAINT probably stems from unwanted hybridization events of R-DNA oligomer imagers with endogenous DNA, and is very abundant in nuclei. While R-DNA-PAINT does not entirely prohibit DNA-PAINT imaging in cellular nuclei[6,19–21], L-DNA-PAINT outperforms R-DNA-PAINT in terms of background staining in cellular domains rich in nucleic acids, which is especially important for single-molecule imaging-based techniques. Super-resolution microscopy of the functional organization of chromosomal DNA and nuclear domains is an important frontier in cell biology[22–24]. L-DNA-PAINT will enable superior investigations of the three-dimensional genome at length scales relevant for the molecular machineries involved in gene activity, DNA repair, splicing and folding, to name but a few[12], both in eukaryotic and prokaryotic organisms. As such, we suggest L-DNA-PAINT as the SMLM method of choice to visualize and quantify DNA-associated molecules at nanoscale resolution specifically, and nuclear structures in general. Finally, L-DNA may generally be a superior labeling agent with which to investigate the nucleus for imaging approaches based on oligomer DNA pairing beyond DNA-PAINT.

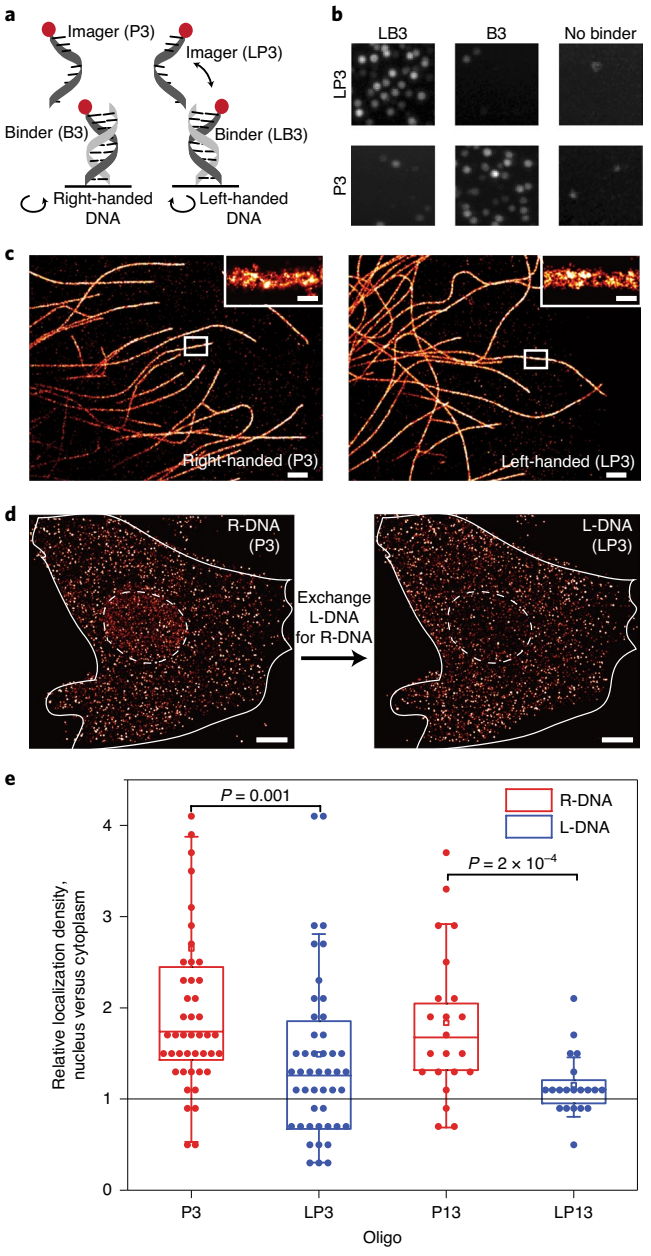

Fig. 1 | Comparison of R-DNA and L-DNA oligomers for DNA-PAINT. **a**, Schematic overview of right- and left-handed DNA-PAINT. Transient hybridization events of fluorophore-labeled right- and left-handed DNA imager oligomers, with their respective binder oligomer temporally immobilizing them for single-molecule localization. **b**, Left-handed (LP3) and right-handed (P3) imager oligomers were added to surface-immobilized left-handed (LB3), right-handed (B3) binder oligos or no oligos, respectively. Right-handed imagers were detected only in the presence of right-handed binders, left-handed imagers only in the presence of left-handed binders. Single-molecule images are 5 × 5 μm^2. **c**, Reconstructed DNA-PAINT images generated from R- and L-DNA-PAINT experiments on immunostained microtubules in HeLa cells. Insets show representative microtubule segments. Scale bars, 1 μm (insets, 100 nm). **d**, Experimental scheme for the detection of nonspecific binding of P3 and LP3 imager strands in nuclei of HeLa cells. Fixed cells were imaged in the presence of P3 and then washed and imaged in the presence of LP3 in identical buffer and at the same concentration. Scale bars, 2 μm. **e**, Plot of relative localization density in the nucleus versus cytoplasm for different imager sequences. Sequence-identical R- and L-DNA imagers are sequentially imaged in the same cell, showing persistent enhancement of nuclear binding in the former. The horizontal line provides visual guidance for equal nuclear and cytoplasmic binding. *P* values were obtained by two-sided paired *t*-tests of 48 cells in ten independent experiments for P3 and LP3, and of 20 cells in two independent measurements for P13 and LP13. In boxplots, center is the median, boxes are interquartile range (IQR) and whiskers are 1.5 × IQR; mean values are represented by open squares.

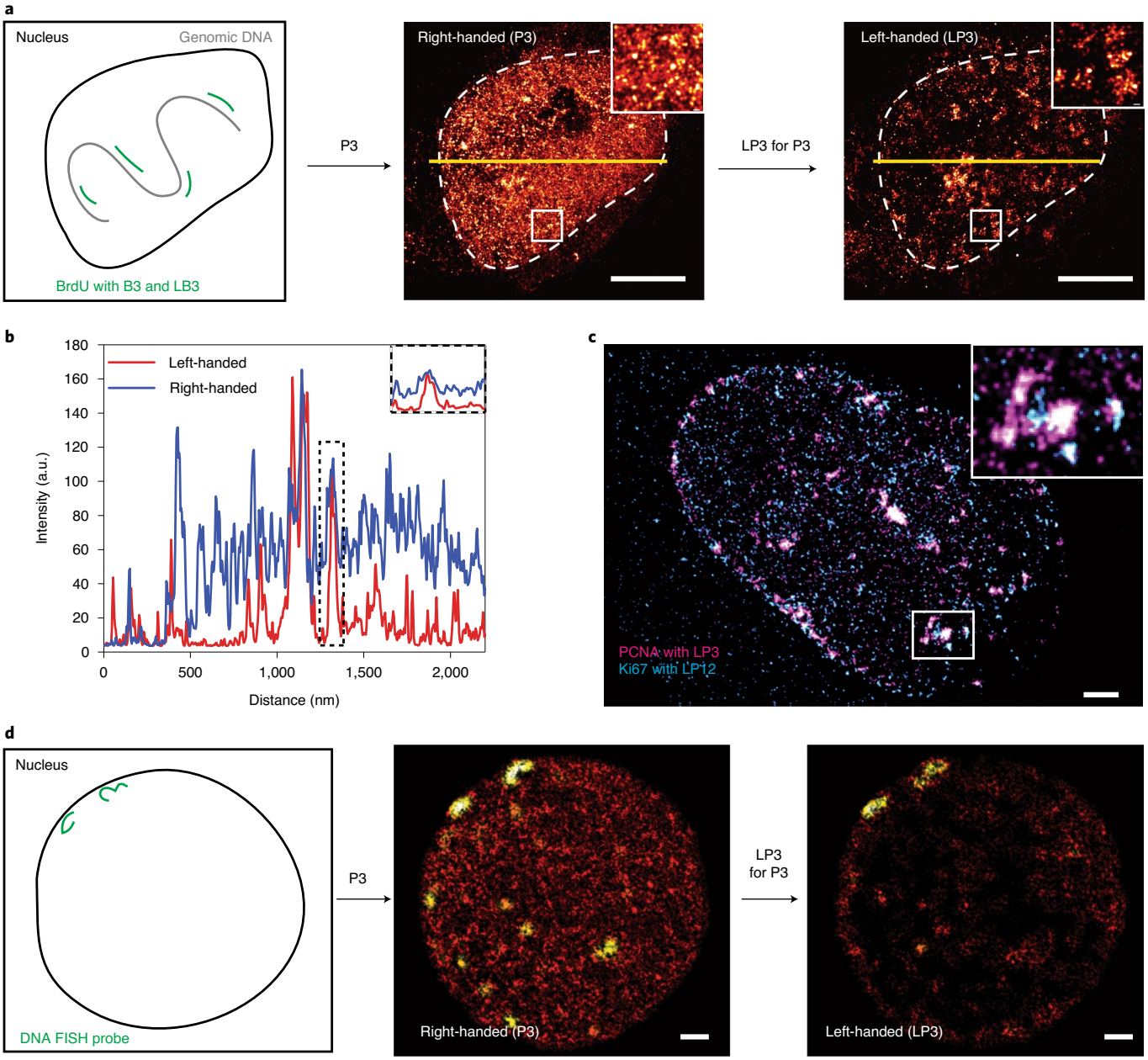

Fig. 2 | Comparison of L- and R-DNA-PAINT for nuclear targets. a, Experimental setup for the imaging of DNA replication foci by incorporation of BrdU into chromosomes. BrdU incorporation sites were stained with a 1:1 mix of B3- and LB3-coupled antibodies and were visualized by both R- and L-DNA-PAINT. **b**, Intensity profiles of a cross-section of the BrdU-stained cell in **a**, colored yellow. The insets show that P3- and LP3-stained cells display the same local maxima, but the background intensity in the latter is notably reduced. **c**, L-DNA-PAINT multiplexing experiment in a HeLa cell nucleus stained with a GFP nanobody, coupled to LB3, directed against overexpressed GFP-PCNA and Ki67 labeled with an antibody linked to LB12. **d**, L-DNA-PAINT FISH experiment on HEK293T cells harboring two copies of an integrated HHV-6A genome. Integrated viral DNA was labeled with an HHV-6A-specific probe, coupled to B3 and LB3 in an equimolar ratio. Subsequent R- and L-DNA-PAINT experiments facilitated the detection of the two viral DNA loci. R-DNA-PAINT via P3 resulted in an increased amount of background localization, hampering the detection of specific FISH loci. Scale bars, 2 µm. a.u., arbitrary units.

Online content

Any methods, additional references, Nature Research reporting summaries, source data, extended data, supplementary information, acknowledgements, peer review information, details of author contributions and competing interests, and statements of data and code availability are available at https://doi.org/10.1038/s41587-020-00753-y.

Received: 8 April 2020; Accepted: 30 October 2020;
Published online: 04 January 2021

References

1. Betzig, E. et al. Imaging intracellular fluorescent proteins at nanometer resolution. *Science* **313**, 1642–1645 (2006).
2. Rust, M. J., Bates, M. & Zhuang, X. Sub-diffraction-limit imaging by stochastic optical reconstruction microscopy (STORM). *Nat. Methods* **3**, 793–796 (2006).
3. Heilemann, M., Margeat, E., Kasper, R., Sauer, M. & Tinnefeld, P. Carbocyanine dyes as efficient reversible single-molecule optical switch. *J. Am. Chem. Soc.* **127**, 3801–3806 (2005).
4. Jungmann, R. et al. Multiplexed 3D cellular super-resolution imaging with DNA-PAINT and Exchange-PAINT. *Nat. Methods* **11**, 313–318 (2014).

5. Schnitzbauer, J., Strauss, M. T., Schlichthaerle, T., Schueder, F. & Jungmann, R. Super-resolution microscopy with DNA-PAINT. *Nat. Protoc.* **12**, 1198–1228 (2017).
6. Schueder, F. et al. Multiplexed 3D super-resolution imaging of whole cells using spinning disk confocal microscopy and DNA-PAINT. *Nat. Commun.* **8**, 2090 (2017).
7. Erdelyi, M. et al. Correcting chromatic offset in multicolor super-resolution localization microscopy. *Opt. Express* **21**, 10978–10988 (2013).
8. Jungmann, R. et al. Quantitative super-resolution imaging with qPAINT. *Nat. Methods* **13**, 439–442 (2016).
9. Jungmann, R. et al. Single-molecule kinetics and super-resolution microscopy by fluorescence imaging of transient binding on DNA origami. *Nano Lett.* **10**, 4756–4761 (2010).
10. Ricci, M. A., Manzo, C., García-Parajo, M. F., Lakadamyali, M. & Cosma, M. P. Chromatin fibers are formed by heterogeneous groups of nucleosomes in vivo. *Cell* **160**, 1145–1158 (2015).
11. Otterstrom, J. et al. Super-resolution microscopy reveals how histone tail acetylation affects DNA compaction within nucleosomes in vivo. *Nucleic Acids Res.* **47**, 8470–8484 (2019).
12. Lakadamyali, M. & Cosma, M. P. Visualizing the genome in high resolution challenges our textbook understanding. *Nat. Methods* **17**, 371–379 (2020).
13. Hauser, N. C. et al. Utilising the left-helical conformation of L-DNA for analysing different marker types on a single universal microarray platform. *Nucleic Acids Res.* **34**, 5101–5111 (2006).
14. Archetti, A. et al. Waveguide-PAINT offers an open platform for large field-of-view super-resolution imaging. *Nat. Commun.* **10**, 1267 (2019).
15. Nieuwenhuizen, R. P. J. et al. Measuring image resolution in optical nanoscopy. *Nat. Methods* **10**, 557–562 (2013).
16. Chagin, V. O. et al. 4D Visualization of replication foci in mammalian cells corresponding to individual replicons. *Nat. Commun.* **7**, 11231 (2016).
17. Osterrieder, N., Wallaschek, N. & Kaufer, B. B. Herpesvirus genome integration into telomeric repeats of host cell chromosomes. *Annu. Rev. Virol.* **1**, 215–235 (2014).
18. Kaufer, B. B. Detection of integrated herpesvirus genomes by fluorescence in situ hybridization (FISH). *Methods Mol. Biol.* **1064**, 141–152 (2013).
19. Beliveau, B. J. et al. Single-molecule super-resolution imaging of chromosomes and in situ haplotype visualization using Oligopaint FISH probes. *Nat. Commun.* **6**, 7147 (2015).
20. Beliveau, B. J. et al. OligoMiner provides a rapid, flexible environment for the design of genome-scale oligonucleotide in situ hybridization probes. *Proc. Natl Acad. Sci. USA* **115**, E2183–E2192 (2018).
21. Frottin, F. et al. The nucleolus functions as a phase-separated protein quality control compartment. *Science* **365**, 342–347 (2019).
22. Gasser, S. M. Nuclear architecture: past and future tense. *Trends Cell Biol.* **26**, 473–475 (2016).
23. Kempfer, R. & Pombo, A. Methods for mapping 3D chromosome architecture. *Nat. Rev. Genet.* **21**, 207–226 (2019).
24. Boettiger, A. N. et al. Super-resolution imaging reveals distinct chromatin folding for different epigenetic states. *Nature* **529**, 418–422 (2016).

Methods

DNA-PAINT oligomers. Binder sequences (B) contained a 5′ biotin or azide modification, and imager sequences (P) were conjugated to Atto655 or Cy3B (P1 only) fluorophores at the 3′ end. In this work, binder sequences (L)B3 and LB12 and imager sequences (L)P1, (L)P3, (L)P12 and (L)P13 were used with the following nucleotide sequences:

Oligo	Nucleotide sequence (3′–5′)	Purchased from
P1-Atto655	Atto655 - CTAGATGTAT	Eurofins Deutschland
P1-Cy3B	Cy3B - CTAGATGTAT	Biomers.net
LP1	CTAGATGTAT	Biomers.net
B3	TTTCTTCATTA	Microsynth AG
LB3	TTTCTTCATTA	Biomers.net
P3	GTAATGAAGA	Eurofins Deutschland
LP3	GTAATGAAGA	Biomers.net
LB12	TTAGTTAGAGC	Biomers.net
P12	GCTCTAACT	Biomers.net
LP12	GCTCTAACT	Biomers.net
P13	CCTTCTCTA	Biomers.net
LP13	CCTTCTCTA	Biomers.net

Coupling of oligomers to nanobodies and antibodies. Binder oligomers were conjugated to secondary donkey anti-mouse antibody (Jackson ImmunoResearch Europe Ltd, catalog no. 715-005-150) as described previously[5]. Briefly, antibodies were labeled with DBCO NHS ester and subsequently conjugated via copper-free click chemistry with azide-modified binder oligos. Green fluorescent protein (GFP) nanobodies were recombinantly expressed and labeled as described previously in great detail[25]. Briefly, his6-tagged anti-GFP nanobodies fused to a C-terminal LPETGG sequence were purified from *Escherichia coli* WK6 with a HisPur cobalt column (Thermo Scientific) and size-exclusion chromatography (Superdex 75 10/300 GL, GE Healthcare). They were then coupled to L-DNA oligomers via Sortase A coupling and copper-free click chemistry and purified over a ZEBA spin desalting column (7 kDa MWCO, Thermo Scientific).

In vitro L- and R-DNA binding assay. Labtek chambers (Ibidi) were cleaned by sonication in 1 M KOH. Then, 0.8 mg ml^{-1} bovine serum albumin (BSA) and 0.2 mg ml^{-1} biotinylated BSA were added to 10 mM Tris-HCl buffer (pH 7.5) supplemented with 100 mM NaCl and 0.05% Tween-20. The sample was incubated with 0.2 mg ml^{-1} streptavidin (Sigma-Aldrich, catalog no. 85878) to allow surface binding to the biotinylated BSA. Next, 500 pM biotinylated LB3 and B3 oligomers were immobilized on streptavidin in 5 mM Tris-HCl buffer (pH 8.0) supplemented with 10 mM $MgCl_2$, 1 mM EDTA and 0.05% Tween-20. The sample was then imaged by titration (ranging from 10 pM to 100 nM) in LP3 or P3 in PBS buffer (pH 8.0) supplemented with 500 mM NaCl.

DNA-PAINT on microtubules in HeLa cells. HeLa cells were plated on 18-mm round coverslips and grown in DMEM (Life Tech) supplemented with 10% fetal calf serum and 1% GlutaMax (Gibco, Thermo Fisher Scientific) at 37 °C in a 5% CO_2 humidified incubator. Before fixation, the cells were washed three times with PEM buffer (0.1 M PIPES pH 6.95, 2 mM EGTA and 1 mM $MgSO_4$) at 37 °C, and permeabilized for 30 s in BRB80 buffer (80 mM PIPES pH 6.8, 1 mM $MgCl_2$ and 10 mM EGTA) supplemented with 0.5% Triton X-100. Next, the cells were fixed in 3.2% paraformaldehyde (PFA) and 0.1% glutaraldehyde in BRB80 buffer. Subsequently, fixation was quenched with 1 mg ml^{-1} $NaBH_4$ in PBS. The sample was then blocked and further permeabilized with 4% goat serum, 1% BSA and 0.1% Triton X-100 in PEM buffer, and subsequently with ImageIT (Thermo Fisher Scientific, catalog no. I36933). The sample was then stained with monoclonal mouse anti-alpha-tubulin antibody (1:1,000; Sigma, no. T5168) and subsequently with goat biotinylated anti-mouse antibody (1:200; polyclonal RU0, BD Pharmingen), followed by the addition of 0.2 mg ml^{-1} streptavidin (Sigma-Aldrich, catalog no. 85878) in PBS. Subsequently, 500 pM biotinylated LB3 or B3 used for the in vitro binding assay was added in PEM buffer. Finally, the sample was imaged with 500 pM LP3 or P3 in PBS supplemented with 500 mM NaCl (also used for the in vitro binding assay).

R- and L-DNA oligomer binding in the nucleus of HeLa cells. HeLa cells were plated as described above. The sample was then washed once with PBS and fixed in 4% PFA in PBS. Subsequently, the sample was washed and quenched with 50 mM NH_4Cl in PBS, followed by blocking and further permeabilization with 4% goat serum, 1% BSA and 0.1% Triton X-100 in PBS buffer and subsequent incubation with ImageIT (Thermo Fisher Scientific, catalog no. I36933). The sample was then imaged with 500 pM L- and R-DNA imagers in PBS supplemented with 500 mM NaCl (also used for the in vitro binding assay).

DNA-PAINT on BrdU incorporation sites in HeLa cells. HeLa cells were plated as described above. To stain replication sites, the growth medium was supplemented with 10 µM BrdU for 1 h and then exchanged for normal growth medium for 1 h. The cells were fixed in 2% PFA in PBS, then permeabilized in 0.2% Triton X-100 in PBS. Next, genomic DNA was denatured by 2 M HCl in PBS. Subsequently, the sample was blocked with 1× BrdU blocking solution (Invitrogen, catalog no. 00-4952-52) and stained overnight with anti-BrdU antibody (1 µg ml^{-1}; clone BU20A, Invitrogen, catalog no. 13-5071-63) in 1× BrdU blocking solution. The sample was stained with streptavidin (0.2 mg ml^{-1}; Sigma-Aldrich, catalog no. 85878) in PBS, then 1 nM of biotinylated LB3 and B3 (as used for the in vitro binding assay) was added. The sample was imaged with 1 nM L- or R-DNA imagers.

L-DNA-PAINT on PCNA and Ki67 in the same HeLa cell. HeLa cells were transfected with GFP-PCNA (Addgene, plasmid no. 105977)[26] by an electroporation method (Neon Transfection System, Thermo Fisher Scientific), plated on 18-mm round coverslips and cultivated in growth medium. The sample was fixed in 4% PFA in PBS and quenched with 50 mM NH_4Cl in PBS. Afterwards, the sample was blocked and permeabilized with 4% goat serum, 1% BSA and 0.1% Triton X-100 in PBS, and subsequently with ImageIT (Thermo Fisher Scientific, catalog no. I36933). The sample was immunostained with anti-Ki67 antibody (1:100; clone B56, BD Pharmigen, catalog no. 556003) and afterwards with GFP nanobody coupled to LB3 (1:100; generated and labeled in house as described in Coupling of oligomers to nanobodies and antibodies) and secondary donkey anti-mouse coupled to LB12 (1:100; for labeling protocol see Coupling of oligomers to nanobodies and antibodies). The sample was imaged in 100 pM LP3 and 1 nM LP12.

DNA-PAINT on HEK293T cells stained with FISH. The integrated HHV-6A genome was detected by FISH as described previously[17], with the following modifications[18,27,28]. Biotin-labeled HHV-6A probes were generated using HHV-6A BAC (strain U1102) and the Biotin-High Prime kit (Sigma-Aldrich). For the classical FISH technique, probes were detected using Cy3-streptavidin (1:1,000; GE healthcare) and DNA was counterstained with DAPI for 10 min (1:3,000; Biolegend). For the FISH technique coupled with the DNA-PAINT approach, probes were stained using streptavidin (0.2 mg ml^{-1}; Sigma-Aldrich, catalog no. 85878) and an equimolar (2 nM) of B3 and LB3, and detected using 2 nM P3 and LP3.

Microscopy. Images were acquired with a Vutara 352 super-resolution microscope (Bruker) equipped with a Hamamatsu ORCA Flash4.0 sCMOS for super-resolution imaging and a 60× oil immersion total internal reflection fluorescence (TIRF) objective (numerical aperture 1.49; ApoN, Olympus), yielding a pixel size of 98 nm. Data were acquired with TIRF/highly inclined and laminated optical sheet-illumination at a laser power density of ~2.5 kW cm^{-2} using a 639-nm laser at room temperature. Figure 1b shows a single image taken at an acquisition time of 300 ms. Figure 1c was reconstructed from 15,000 images taken at an acquisition time of 300 ms, represented by Picasso software with the hot color map and global localization precision. Figures 1d and 2a were reconstructed from 5,000 image frames taken at an acquisition time of 100 ms, represented by Picasso software (v.0.2.8; https://github.com/jungmannlab/picasso) with the hot color map and individual localization precision with 0.3 pixels isotropic. For Fig. 2c, an overlap of 5,000 frames (100 ms acquisition time) taken with LP3 and LP12 was generated in Fiji (ImageJ v.1.52t, GNU General Public License) using the TurboReg Plugin[29]. Figure 2d was reconstructed using Vutara's SRX software v.6.04.14 and is represented by pair correlation of localizations with the heat look-up table.

Statistics and reproducibility. For Fig. 2a, BrdU staining was performed on 11 cells in three independent experiments, all showing significantly higher localization density for R-DNA-PAINT in the nucleus. For Fig. 2c, multiplexing experiments were performed for three cells in one dependent experiment, all showing discrete staining for those targets. For Fig. 2d, the FISH experiments were undertaken with 30 cells in five independent experiments, in which we twice detected two integration sites owing to spatial separation of the sites and, as such, low probability of detecting both of them in the same focal plane. Statistical analysis was performed in OriginPro 2017G 64-bit.

Reporting Summary. Further information on research design is available in the Nature Research Reporting Summary linked to this article.

Data availability

The microscopy data that support the findings of this study will be available from the corresponding author upon reasonable request, due to storage limitations. Source data are provided with this paper.

References

25. Fabricius, V., Lefèbre, J., Geertsema, H., Marino, S. F. & Ewers, H. Rapid and efficient C-terminal labeling of nanobodies for DNA-PAINT. *J. Phys. D: Appl. Phys.* https://doi.org/10.1101/389445 (2018).
26. Icha, J., Kunath, C., Rocha-Martins, M. & Norden, C. Independent modes of ganglion cell translocation ensure correct lamination of the zebrafish retina. *J. Cell Biol.* **215**, 259–275 (2016).

27. Saviola, A. J. et al. Chromatin profiles of chromosomally integrated human herpesvirus. *Front. Microbiol.* https://doi.org/10.3389/fmicb.2019.01408 (2019).
28. Wallaschek, N. et al. The telomeric repeats of human herpesvirus 6A (HHV-6A) are required for efficient virus integration. *PLoS Pathog.* https://doi.org/10.1371/journal.ppat.1005666 (2016).
29. Thévenaz, P., Ruttimann, U. E. & Unser, M. A pyramid approach to subpixel registration based on intensity. *IEEE Trans. Image Process.* **7**, 27–41 (1998).

Acknowledgements

We thank all members of the Ewers laboratory for helpful discussions. This study was supported by the ERC (starting grant no. Stg 677673 awarded to B.B.K.) and Deutsche Forschungsgemeinschaft (project no. 278001972 - TRR 186 and SFB 958 to H.E.).

Author contributions

H.J.G. and H.E. developed the initial workflow, conceived the project and established the L-DNA-PAINT approach. G.A. conducted the FISH experiments. V.F. synthesized and labeled the left-handed nanobody and secondary antibody. H.J.G. acquired and analyzed the data. H.J.G. and H.E. wrote the manuscript. G.A. and B.B.K. edited the manuscript. B.B.K. offered guidance and resources for the project. H.E. supervised the project. All authors have reviewed and approved the manuscript.

Competing interests

The authors declare no competing interests.

Additional information

Extended data is available for this paper at https://doi.org/10.1038/s41587-020-00753-y.

Supplementary information is available for this paper at https://doi.org/10.1038/s41587-020-00753-y.

Correspondence and requests for materials should be addressed to H.E.

Peer review information *Nature Biotechnology* thanks the anonymous reviewers for their contribution to the peer review of this work.

Reprints and permissions information is available at www.nature.com/reprints.

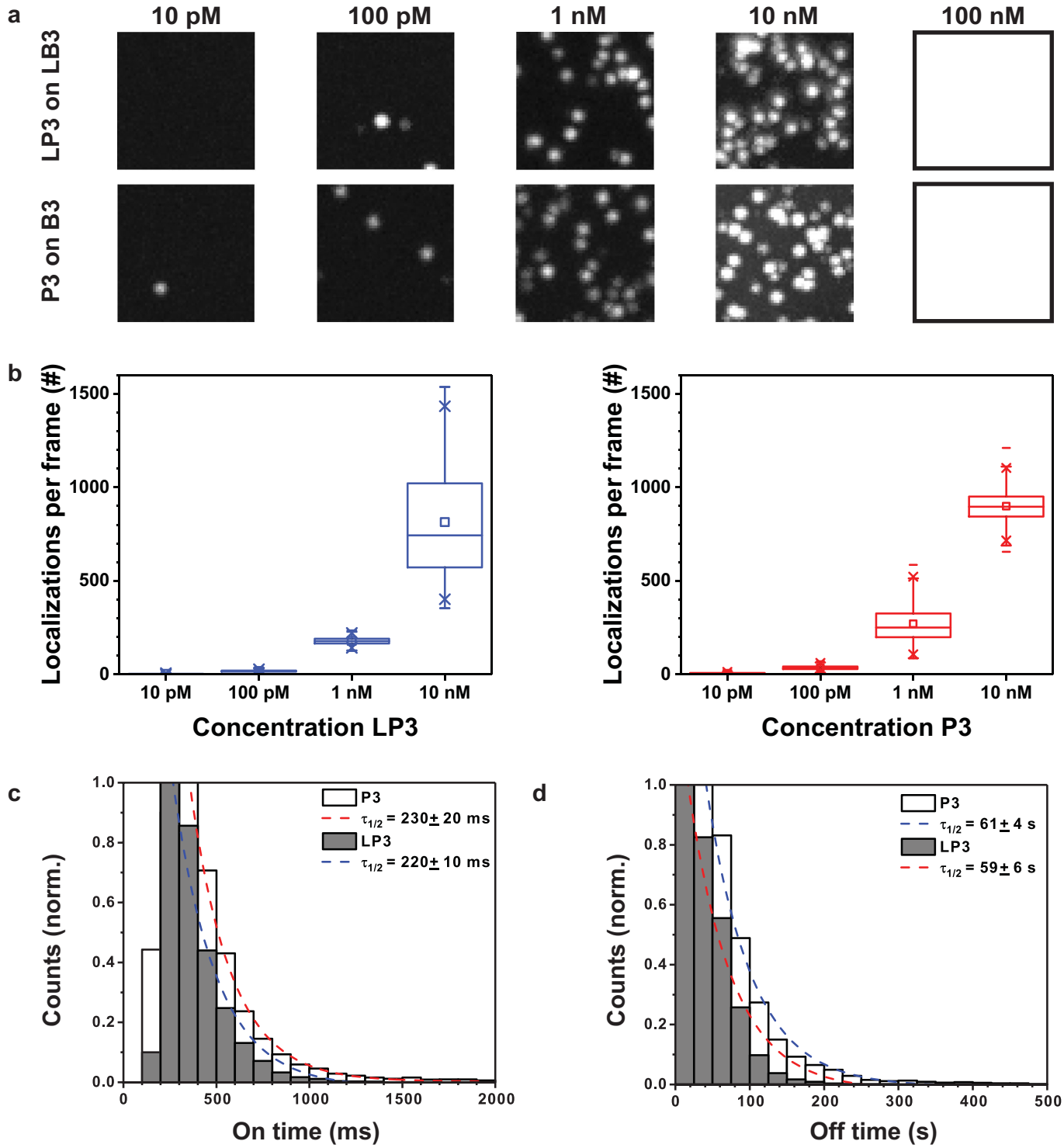

Extended Data Fig. 1 | Kinetics of L-DNA and R-DNA PAINT. a, Titration experiment of L-DNA imagers (LP3) on L-DNA binders (LB3) and R-DNA imagers (P3) on R-DNA binders (LB3). Single molecule images are 5 µm x 5 µm. **b**, Plot of total number of localizations per frame in the titration experiment was quantified for L- and R-DNA and found to be very similar. No single molecules were detected for 100 nM of imagers and as such excluded from these graphs. Boxplots (centre is the median; box are the IQR; whiskers are 1.5 × IQR; mean values are represented by open squares; X represent the 1% and 99% percentiles). **c**, Fluorescence on-times as a result of imager-binder hybridization were extracted. The histogram represents the distribution of on-times for R-DNA and L-DNA and was fitted with a single exponential, yielding a half time of 230 ± 20 ms and 220 ± 10 ms, respectively. Data were gathered from 3 independent measurements. **d**, The time between subsequent imager-binder hybridization event is defined as the off-time. For 1 nM of imager, the off-times were found to be 61 ± 4 s and 59 ± 6 s for R- and L-DNA, respectively. Data were gathered from 3 independent measurements.

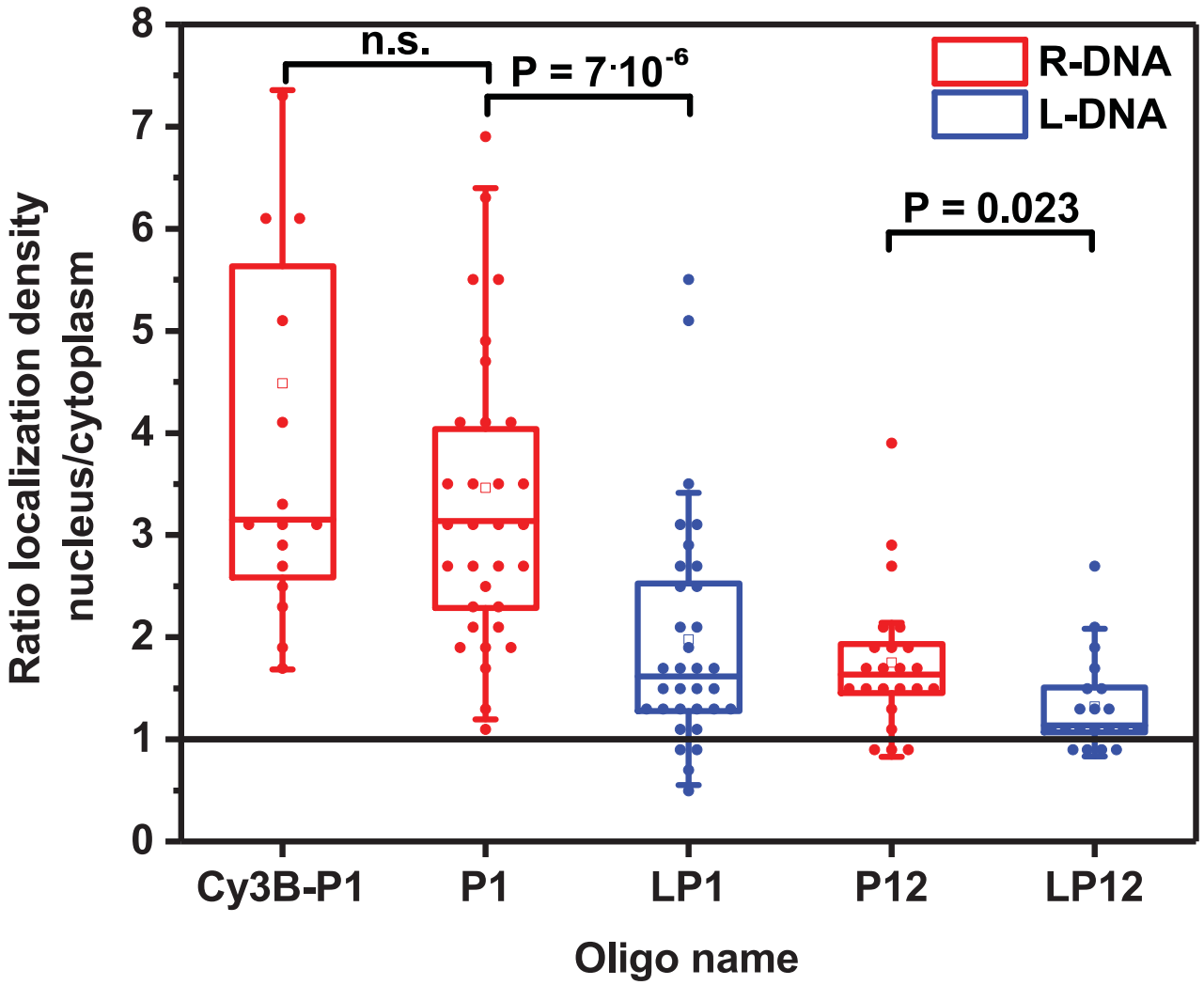

DNA oligo name	Nucleotide sequence (5'-3')	Mean localization density nucleus/cytoplasm ± S.E.M.
(L)P1	CTAGATGTAT	LP1: 2.0 ± 0.2, P1: 3.5 ± 0.9
(L)P3	GTAATGAAGA	LP3: 1.5 ± 0.1, P3: 2.7 ± 0.4
(L)P12	GCTCTAACT	LP12: 1.3 ± 0.1, P12: 1.8 ± 0.2
(L)P13	CCTTCTCTA	LP13: 1.2 ± 0.1, P13: 1.9 ± 0.2

Extended Data Fig. 2 | Nuclear localization density is enhanced by R-DNA imagers. P1 and LP1 as well as P12 and LP12, that are coupled to an Atto655 fluorophore, show a significant difference in the ratio of localization density in the nucleus over the cytoplasm. No significant difference was detected between Atto655 or Cy3B as fluorescent dyes. P-values are obtained from two-sided paired t-Tests 16 cells stained with Cy3B-P1 and 33 cells for P1 and LP1 in 3 independent experiments and 20 cells in 2 independent measurements for P13 and LP13. Boxplots (center is the median; box are the IQR; whiskers are 1.5 × IQR; mean values are represented by open squares).

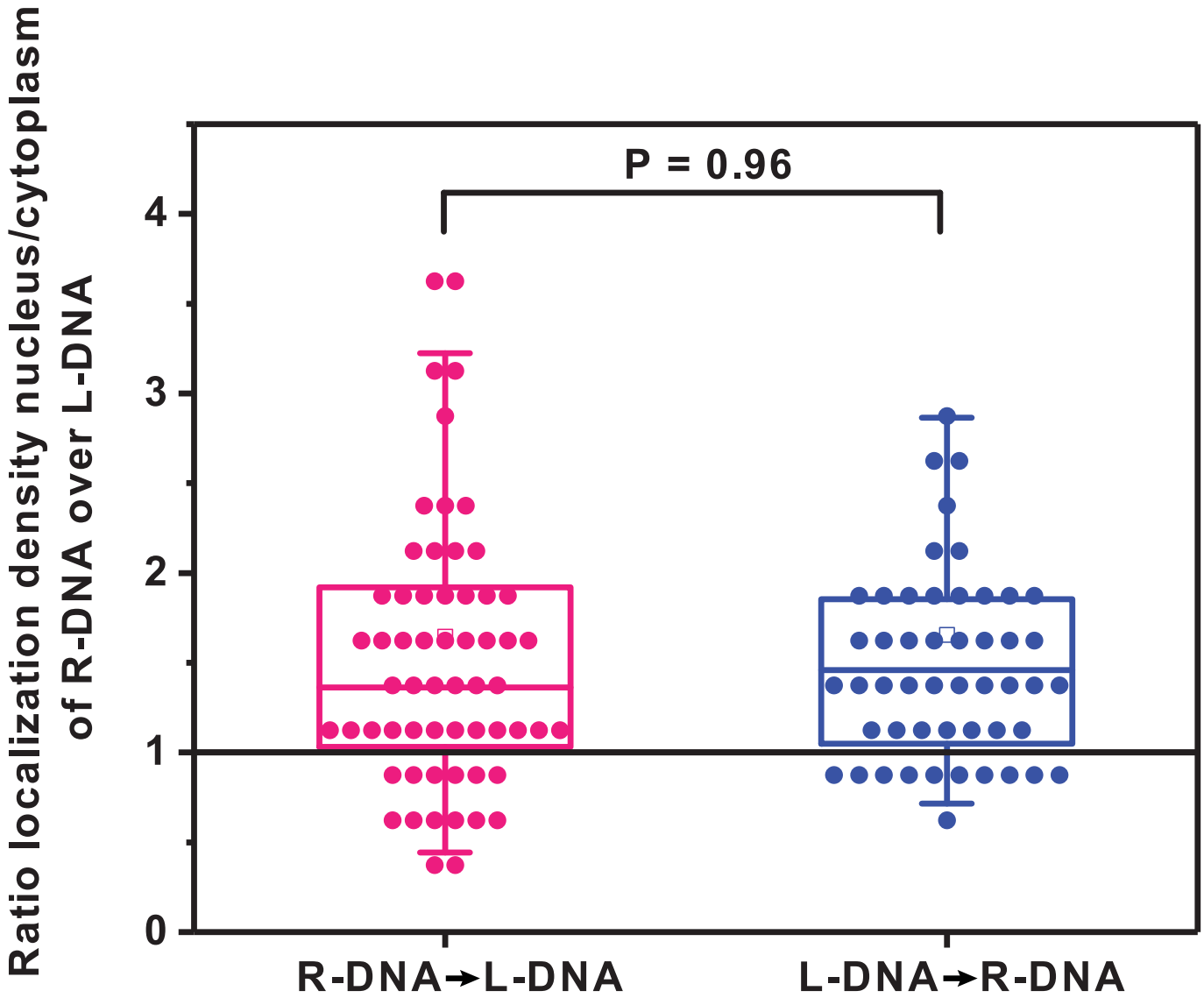

Extended Data Fig. 3 | Plot of relative localization density of R-DNA over L-DNA for multiplexing experiments initiated with either R-DNA or L-DNA. Cells were imaged with sequence-identical R-DNA and L-DNA imagers, sequentially. No significant difference in the relative localization densities of R-DNA over L-DNA was found when the image sequence was initiated with R-DNA (pink) or L-DNA (blue). P-value was obtained by two-tailed *t*-test of 61 and 52 cells for R-DNA and L-DNA initiation, respectively, in 17 independent experiments. Boxplots (centre is the median; box are the IQR; whiskers are 1.5 × IQR; mean values are represented by open squares).

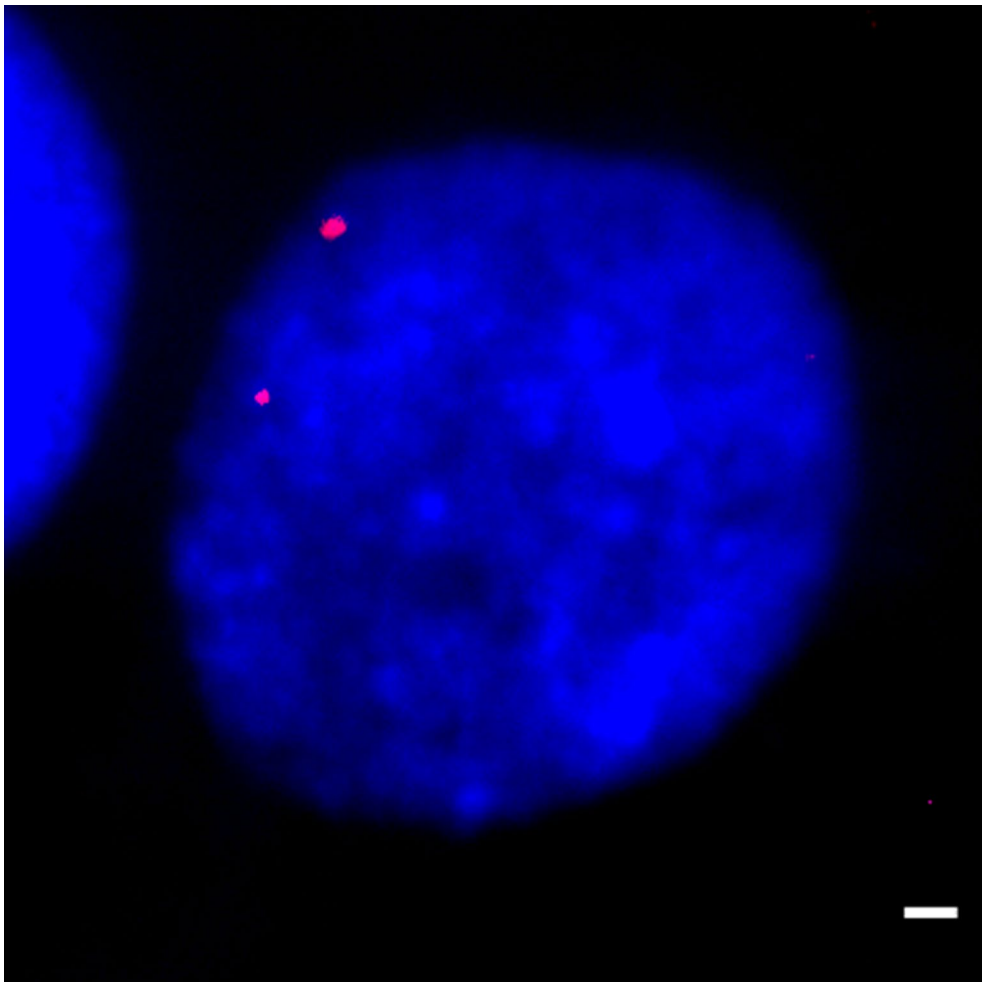

Extended Data Fig. 4 | Detection of integrated HHV-6A genomes by FISH. FISH was performed on HEK293T cells harboring two copies of an integrated HHV-6A genome as described previously[18]. The two viral integration sites were detected in the cell nuclei using HHV-6A specific probes by FISH, matching the detection using the DNA-PAINT approach, and could be successfully reproduced in 30 independent FISH experiments. Scale bar is 2 µm.

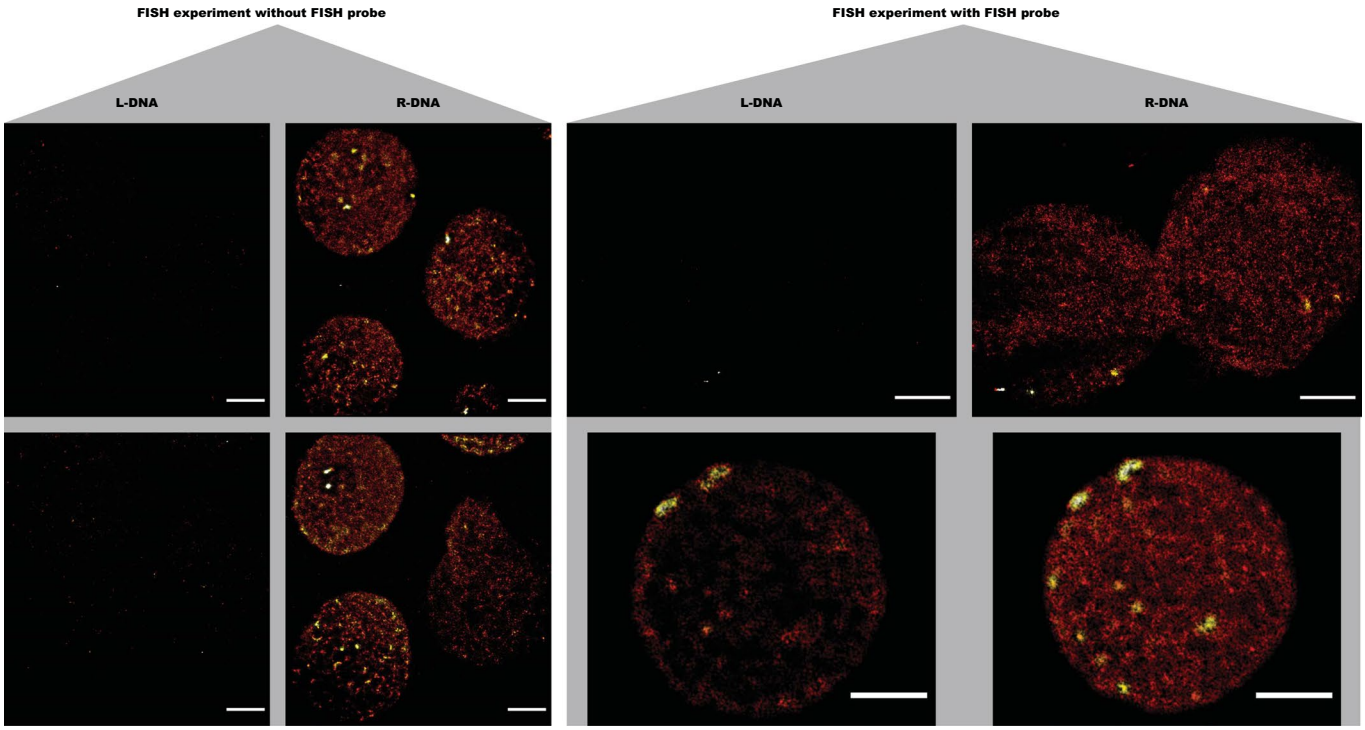

Extended Data Fig. 5 | Localization of R-DNA and L-DNA imagers in the nucleus of FISH samples. R-DNA imagers strongly localize to the nucleus of FISH samples, both without DNA-FISH probes and with DNA-FISH probes coupled to complementary R-DNA binders. L-DNA imagers are not detected in the FISH samples omitting the FISH probes, but show specific loci where the samples are labeled with DNA-FISH probes. Scale bars are 5 μm. All images are reconstructed from 5000 frames and 2 nM imager concentrations.

nature research

Corresponding author(s): Helge Ewers

Last updated by author(s): Oct 26, 2020

Reporting Summary

Nature Research wishes to improve the reproducibility of the work that we publish. This form provides structure for consistency and transparency in reporting. For further information on Nature Research policies, see Authors & Referees and the Editorial Policy Checklist.

Statistics

For all statistical analyses, confirm that the following items are present in the figure legend, table legend, main text, or Methods section.

n/a	Confirmed	
☐	☒	The exact sample size (*n*) for each experimental group/condition, given as a discrete number and unit of measurement
☐	☒	A statement on whether measurements were taken from distinct samples or whether the same sample was measured repeatedly
☐	☒	The statistical test(s) used AND whether they are one- or two-sided *Only common tests should be described solely by name; describe more complex techniques in the Methods section.*
☒	☐	A description of all covariates tested
☒	☐	A description of any assumptions or corrections, such as tests of normality and adjustment for multiple comparisons
☐	☒	A full description of the statistical parameters including central tendency (e.g. means) or other basic estimates (e.g. regression coefficient) AND variation (e.g. standard deviation) or associated estimates of uncertainty (e.g. confidence intervals)
☐	☒	For null hypothesis testing, the test statistic (e.g. *F*, *t*, *r*) with confidence intervals, effect sizes, degrees of freedom and *P* value noted *Give P values as exact values whenever suitable.*
☒	☐	For Bayesian analysis, information on the choice of priors and Markov chain Monte Carlo settings
☒	☐	For hierarchical and complex designs, identification of the appropriate level for tests and full reporting of outcomes
☒	☐	Estimates of effect sizes (e.g. Cohen's *d*, Pearson's *r*), indicating how they were calculated

Our web collection on statistics for biologists contains articles on many of the points above.

Software and code

Policy information about availability of computer code

Data collection	Data was collected on a Vutara 352 System (Bruker 2020) using Vutara's SRX software 6.04.14.
Data analysis	For figure 1b, we used Fiji (ImageJ 1.52t, GNU General Public License) to cut out a selection from the raw data. For Figure 1c, 1d, 2a and c, Picasso software has been used (Version 0.2.8, https://github.com/jungmannlab/picasso). The localization densities in Figure 1e are calculated by the Vutara SRX software 6.04.14. Figure 1e, 2b and Extended data Figures 1, 2 and 3 were prepared with OriginPro 2017G 64-Bit. Figure 2d and Extended data Figure 5 were analyzed with Vutara SRX software 6.04.14 (Bruker 2020).

For manuscripts utilizing custom algorithms or software that are central to the research but not yet described in published literature, software must be made available to editors/reviewers. We strongly encourage code deposition in a community repository (e.g. GitHub). See the Nature Research guidelines for submitting code & software for further information.

Data

Policy information about availability of data

All manuscripts must include a data availability statement. This statement should provide the following information, where applicable:

- Accession codes, unique identifiers, or web links for publicly available datasets
- A list of figures that have associated raw data
- A description of any restrictions on data availability

A reporting summary for this Article is available as Extended data file. Statistical source data are provided with this paper. The microscopy data that support the findings of this study will be available from the corresponding author upon reasonable request due to storage limitations.

Field-specific reporting

Please select the one below that is the best fit for your research. If you are not sure, read the appropriate sections before making your selection.

☒ Life sciences ☐ Behavioural & social sciences ☐ Ecological, evolutionary & environmental sciences

For a reference copy of the document with all sections, see nature.com/documents/nr-reporting-summary-flat.pdf

Life sciences study design

All studies must disclose on these points even when the disclosure is negative.

Sample size	In vitro hybridization assay data (Fig 1b and Extended data Fig. 1) were required from three independent measurements in triple, resulting in 1000s of datapoints per measurement. Microtubules were visualized in 5 and 4 cells for L-DNA-PAINT and R-DNA-PAINT (Fig 1c), giving an average microtubule diameter of 39 and 33 nm, of 22 and 9 microtubule regions respectively, which corresponds well to previous reports. In Figure 1e, the localization densities of 48 cells for P3 and LP3 and 20 cells for P13 and LP13 are compared. According to a paired T-test calculated by Origin Pro, the difference in mean value was significant. BrdU stainings were detected for 11 cells, which all showed an enrichment in R-DNA localizations in comparison to the L-DNA localizations. To show the multiplexing ability, we performed Ki67 and PCNA detection in the same cell for 3 cells, all showing discrete stainings as was published before. To illustrate the strength of L-DNA-PAINT, we show one FISH staining which shows the two integration sites of the HHV in the HEK293T genome in Figure 2d and one more in Extended data Fig. 5.
Data exclusions	No data was excluded.
Replication	In vitro hybridization assay (Fig 1b and Extended Fig. 1) was performed in triplet, the hybridization kinetics of L- and R-DNA were reproducible during those 3 experiments. Microtubules were visualized in 5 and 4 cells for L-DNA-PAINT and R-DNA-PAINT, respectively (Fig 1c), yielding a comparable microtubule diameter and Fourier ring correlation. For the hybridization of imagers in the nucleus, we measured 48 cells in 10 independent experiments for P3 and LP3 and 20 cells in 2 independent measurements for P13 and LP13 (Fig. 1e). We performed BrdU stainings on 11 cells in total, all of them showed the significant higher localization density for R-DNA-PAINT in the nucleus. The Ki67 and PCNA stainings in Hela cells were performed in triple, all of them allowed us to visualize the discrete stainings for those targets. The FISH experiments were undertaken for 30 cells, of which we could detect the two integration sites only twice due to the spatial separation of the integration sites and as such a low probability to detect both of them in the same image plane.
Randomization	For all experiments, despite Figure 1c, we performed interdependent experiments on the same cells (since we performed both left- and right-handed PAINT experiments on the same cell). As such, samples intrinsically were not allocated in separated groups.
Blinding	Localization densities were determined by the Vutara SRX software and as such we renounced from blinding.

Reporting for specific materials, systems and methods

We require information from authors about some types of materials, experimental systems and methods used in many studies. Here, indicate whether each material, system or method listed is relevant to your study. If you are not sure if a list item applies to your research, read the appropriate section before selecting a response.

Materials & experimental systems

n/a	Involved in the study
☐	☒ Antibodies
☐	☒ Eukaryotic cell lines
☒	☐ Palaeontology
☒	☐ Animals and other organisms
☒	☐ Human research participants
☒	☐ Clinical data

Methods

n/a	Involved in the study
☒	☐ ChIP-seq
☒	☐ Flow cytometry
☒	☐ MRI-based neuroimaging

Antibodies

Antibodies used	Monoclonal Mouse anti-alpha-tubulin (Clone B-5-1-2, Sigma-Aldrich, T5168), Polyclonal Goat biotinylated anti-mouse antibody (BD Biosciences, Pharmingen, Catalog Nr. 550337), Biotinylated Anti-BrdU antibody (Clone BU20A, only available in the eBiosciences BrdU kit for IHC/ICC Colorimetric, Invitrogen, Thermo Scientific, Cat Nr. 8800-6599), Purified Mouse Anti-Ki67 (Clone B56, BD Biosciences, Pharmingen, Cat Nr. 556003) and donkey anti-mouse antibody (Jackson ImmunoResearch Europe Ltd, Cat. Nr. 715-005-150) were used in this study.
Validation	Anti-tubulin was validated by Sigma-Aldrich for indirect immunofluorescence on cultured human and chicken fibroblasts and have been used by our laboratory for super-resolution microscopy on Ptk2 cells (Ries et al. Nature Methods 2012). Biotinylated anti-mouse antibody was tested for ELISA and frozen, paraffin, and zinc-fixed immunohistochemistry by BD Pharmingen TM. Anti-Ki67 antibodies are regularly tested for intracellular staining and bioimaging of Hela, A549 and U2OS cells by BD Pharmingen

TM. The Anti-BrdU BU20A antibody has been tested by intracellular staining and flow cytometric analysis of BrdU-labeled mouse splenocytes by eBiosciences.

Eukaryotic cell lines

Policy information about cell lines

Cell line source(s)	HeLa ATCC CCL2 and 293T ATCC CRL-3216
Authentication	The Hela cell lines used were not authenticated, the epithelial phenotype was confirmed for the 293T cells.
Mycoplasma contamination	The cells used in this study were tested negative for mycoplasma contamination.
Commonly misidentified lines (See ICLAC register)	None used in this study